Fluid Dynamics & Materials Processing

Tech Science Press

Doi:10.32604/fdmp.2025.065459

ARTICLE

Evaluation of Tubing Integrity with Rectangular Corrosion under Thermo-Chemical-Mechanical Coupling

Yi Huang[1,*], Ming Luo[1], Zhujun Li[1], Donglei Jiang[1], Ping Xiao[1], Mingyuan Yao[2] and Jia He[2]

[1]CNOOC Co., Ltd. Hainan Branch, Hainan, 570100, China

[2]State Key Laboratory of Oil and Gas Reservoir Geology and Exploitation, Southwest Petroleum University, Chengdu, 610500, China

*Corresponding Author: Yi Huang. Email: 13060058004@163.com

Received: 13 March 2025; Accepted: 21 June 2025; Published: 12 September 2025

ABSTRACT: This study presents a comprehensive mechanical analysis of P110S oil tubing subjected to thermal and chemical coupling effects, with particular attention to the presence of rectangular corrosion defects. Drawing on the material's stress–strain constitutive behavior, thermal expansion coefficient, thermal conductivity, and electrochemical test data, the research incorporates geometric nonlinearities arising from large deformations induced by corrosion. A detailed three-dimensional finite element (FE) model of the corroded P110S tubing is developed to simulate its response under complex loading conditions. The proposed model is rigorously validated through full-scale burst experiments and analytical calculations based on theoretical formulations. Building upon this validation, the Extended Finite Element Method (XFEM) and a failure criterion grounded in damage evolution mechanics are applied to investigate the mechanical behavior of the tubing under the coupled influences of temperature, stress, and chemical corrosion. Special emphasis is placed on the role of rectangular corrosion features in determining failure mechanisms. To further elucidate the impact of multiple interacting parameters, a sensitivity analysis is performed by integrating grey correlation theory with simulation outcomes. Based on these findings, the study systematically explores the elastic–plastic deformation process, crack initiation and propagation behavior, and the burst failure response of tubing specimens with varying axial lengths and depths of corrosion. The proposed methodology provides a robust predictive framework for petroleum engineers to evaluate fracture pressure, diagnose failure modes, assess operational risks, and optimize production strategies.

KEYWORDS: Tubing corrosion; XFEM; multi-field coupling; burst failure; service life

1 Introduction

CCUS (CO_2 capture, utilization, and storage) and CO_2-EOR (CO_2 enhanced oil displacement) technologies are widely used globally. CO_2 flooding has many advantages, including significantly enhancing oil recovery with low cost. However, the combination of concentrated CO_2 and free water inevitably causes severe CO_2 corrosion of tubing steel, threatening oil and gas production safety. Severe corrosion can lead to tubing failure, substance leaks, economic losses, environmental pollution, and even fatalities [1–3].

At present, many scholars have carried out a lot of research in the field of corrosion defect assessment in the world. Sedmak et al. [4] have revealed the impact of geometric features on the residual strength of the J55 casing and verified the ASME B31G standard for predicting failure pressure by using experiments and simulation. A three-dimensional numerical model of the tubing has been constructed by Mondal and Dhar [5,6] based on fracture mechanics theory, which provides a new means for the visual analysis of the dynamic failure process. The multiple regression model has been established by Fahed et al. and Heggab

et al. [7,8] for rapid engineering assessment of tubing. The mechanical model with longitudinal rectangular cracks was developed by Okodi et al. [9–12], which can provide an important reference for the revision of industry standards. The equivalent stress of tubing with rectangular corrosion defect under internal pressure has been investigated by Cao and Yang [13–17], by which the relationship between the maximum equivalent stress and the length and depth of corrosion defect has been revealed. A numerical simulation model of tubing with corrosion defects has been established by Chen et al. [18–21] to analyze the influence of different parameters on collapse pressure, by which the safety assessment system under multi-defect conditions has been presented. The distribution and variation of equivalent stress for high-grade steel tubing have been investigated by Olatunde et al. [21–24]. The structure integrity of tubing with corrosion defect under thermo-mechanical coupling has been investigated by Soares et al. [25] based on FEM, by which the interaction mechanism between temperature and stress has been revealed. The FEM model of a pipeline with corrosion defect has been created by Feki et al. [26–28], under mechanical-chemical coupling to predict corrosion parameters. A nonlinear 3D thermal-mechanical coupling model has been presented by Deng et al. [29] to simulate the burst behavior of corroded tubing. In conclusion, those models and methods can provide important references for failure analysis and safety assessment of corroded tubing.

Although many studies on the failure analysis of tubing with corrosion defects have been carried out by many predecessors, the current research mainly focuses on static analysis. On the basis of the previous researchers, the dynamic simulation method has been presented based on the actual corrosion behavior of downhole tubing, by which the three-dimensional dynamic mechanical model has been established under the thermal-mechanical-chemical multi-field coupling by developing the stress-corrosion subroutine. This method has significant advantages with due consideration of the interactive effect among the corrosion rate, evolving structural morphology in the corrosion region, and stress distribution with service time.

2 Mechanical and Thermodynamic Parameters of Tubing

The mechanical and thermal properties of P110S tubing has been measured following the national standards [30,31]. The tensile performance test has been conducted by an MTS machine, the thermal expansion coefficient test was conducted by a NETZSCH DIL 402C thermal expansion instrument, and the thermal conductivity test was conducted by an LFA427 laser thermal conductivity meter. Based on those tests, the stress-strain constitutive relationship, thermal expansion coefficient, and thermal conductivity of P110S tubing material are obtained. The specific test results are shown in Fig. 1. The main chemical composition of P110S tubing is as follows: w(Mn) = 1.29%, w(Cr) = 0.50%, w(Si) = 0.35%, w(C) = 0.23%, w(P) = 0.01%, w(S) = 0.01%, w(Mo) = 0.11%, w(Ni) = 0.07%, and the remaining is w(Fe).

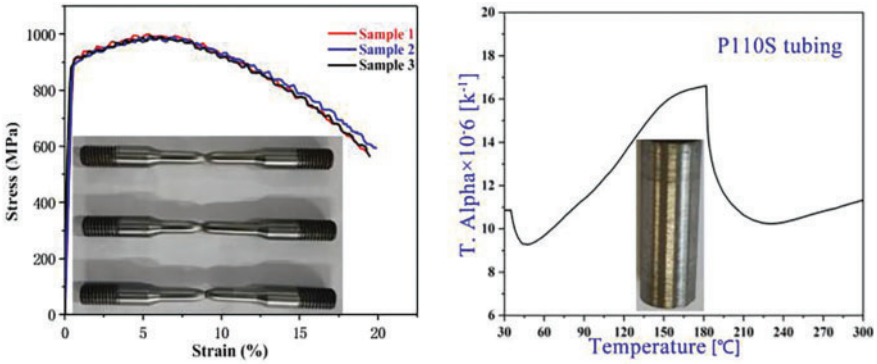

(**a**) Stress-strain constitutive relationship (**b**) Coefficient of thermal expansion

Figure 1: (Continued)

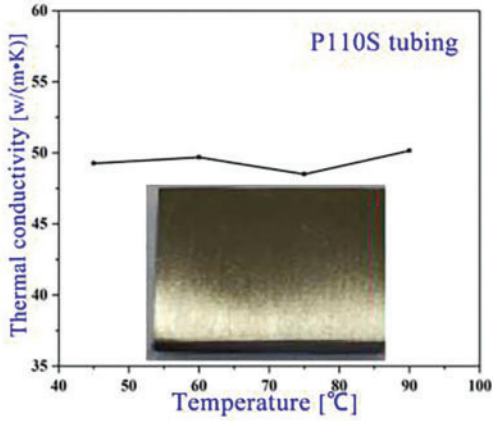

(**c**) Thermal conductivity

Figure 1: Thermodynamic properties of P110S tubing

3 Numerical Model

The three-dimensional mechanical model of corroded tubing with rectangular corrosion defect under thermal-mechanical-chemical multi-field coupling has been established by using the nonlinear finite element method with due consideration of the geometric non-linearity caused by large deformation. The influence of thermal-mechanical-chemical multi-field coupling on damage evolution has been investigated by the user-defined mechanical-chemical damage control subroutine (S-C-UMESHMOTION) and adaptive grid technology (Arbitrary Lagrangian-Eulerian, ALE). The subroutine does not alter the original stress and strain distribution during the node position adjustment process. Due to this characteristic, the subroutine can be used for wear and ablation simulation. To a certain extent, corrosion could be regarded as a special 'abrasion'. Therefore, it is feasible and scientific to apply this subroutine in tubing corrosion simulation. Simultaneously, the extended finite element (XFEM) method in ABAQUS has been employed to simulate crack initiation and propagation of corroded tubing under internal pressure.

3.1 Classification and Standardization of Corrosion Defects

(1) Classification of corrosion defects

Due to the complex service environment, there are many reasons for tubing corrosion, but the corrosion morphology of tubing is mainly divided into three types, including uniform corrosion, localized corrosion, and pitting. Uniform corrosion and localized corrosion are the most common, and they mainly reduce the service life and strength of tubing, and localized corrosion can lead to the perforation of tubing too. Pitting corrosion mainly produces stress concentration and leads to perforation and fracture of tubing [32,33]. In this paper, the mechanical behavior of tubing with uniform corrosion and local corrosion of tubing is the focus of investigation.

(2) Standardization of corrosion defects

The corrosion defects on the tubing surface are complex and random in shape and size, which makes it challenging to quantitatively characterize their geometric parameters. In this study, the regularization method for local wall thinning defects proposed in GB/T 19624-2019 is adopted to simplify localized corrosion defects. It has been demonstrated that the simplified model has no impact on the engineering results [34,35]. Uniform corrosion and localized corrosion are equivalently modeled as rectangular defects

with equal depth. The rotary cutting method is employed in three-dimensional modeling to generate equal-depth rectangular corrosion on the inner wall of tubing [34]. The simplified schematic diagram is presented in Fig. 2.

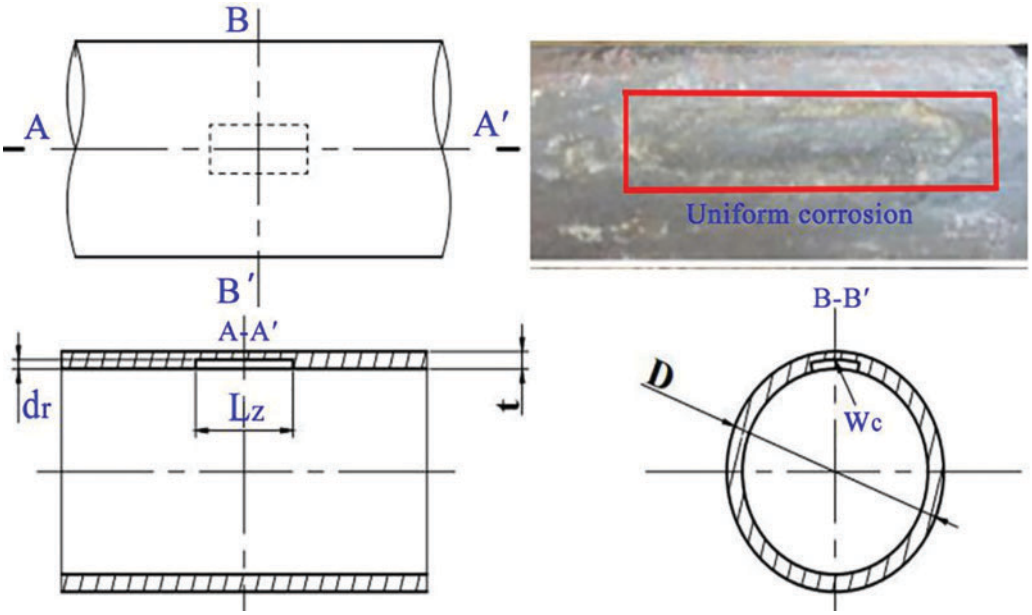

Figure 2: Schematic diagram of a simplified rectangular concave model of equal depth

3.2 Establishment of Finite Element Model of P110S Tubing

(1) Model parameters of P110S tubing

Based on the test results, the geometric, mechanical, and thermodynamic parameters of the P110S tubing material are shown in Table 1. To eliminate boundary effects, the tubing length is set to 500 mm based on the Saint-Venant principle. A three-dimensional geometric model of the P110S tubing is established by using SolidWorks software, as shown in Fig. 3a.

Table 1: Geometrical and mechanical parameters of P110S tubing

External diameter (mm)	Wall thickness (mm)	Yield strength (MPa)	Tensile strength (MPa)	Elasticity modulus (GPa)	Poisson ratio	Thermal conductivity (K^{-1})	Coefficient of Thermal expansion ($W\cdot(m\cdot K)^{-1}$)
88.9	6.45	895	990	210	0.3	$1.0 * 10^{-6}$	49.4

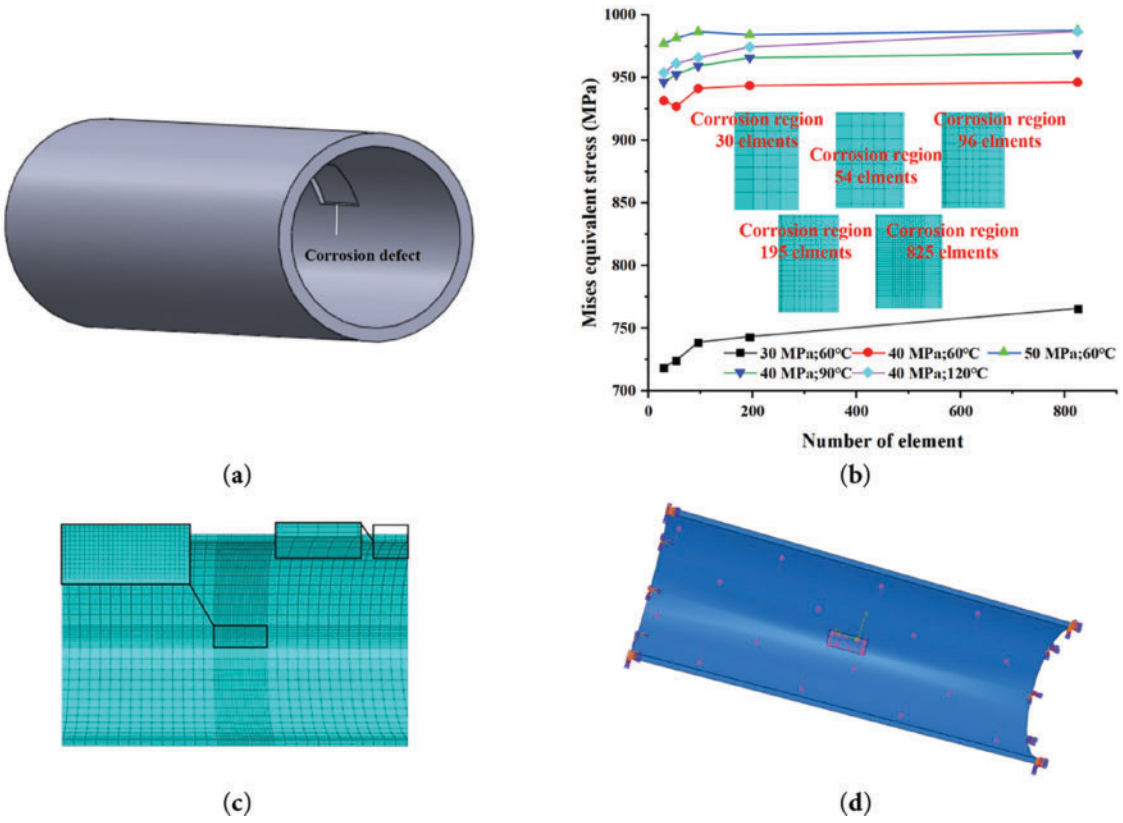

Figure 3: Geometric model and mechanical model. (**a**) 3D model diagram of P110S tubing with rectangular corrosion defect; (**b**) Mesh sensitivity analysis; (**c**) Meshing of P110S tubing with rectangular corrosion defects; (**d**) P110S tubing boundary condition setting

(2) Element meshing

In finite element simulations, the mesh quality is an important factor that directly affects computational accuracy. Generally, a higher number of mesh elements improves the precision of results, but it also increases computational time. Therefore, reasonable element meshing and scientific validation are key to ensuring simulation accuracy. Fig. 3b and Table 2 show that the mesh quality and simulation accuracy could meet the requirements by adopting the mesh density with 195 elements in the corrosion area, by which the axial length of corrosion regions is partitioned into 13 segments, the circumferential length was split into 5 sections, and the radial thickness is divided into 3 layers, as shown in Fig. 3c.

Table 2: Mesh sensitivity analysis

Number of element	Pressure (MPa)	Mises equivalent stress (MPa)	Pressure (MPa)	Mises equivalent stress (MPa)	Pressure (MPa)	Mises equivalent stress (MPa)
30	30	718.5	40	931.4	50	976.8
54	30	724.1	40	926.7	50	981.3
96	30	738.6	40	941.2	50	986.4
195	30	743.1	40	943.5	50	984
825	30	765.5	40	946.2	50	987.6

(Continued)

Table 2 (continued)

Number of element	Pressure (MPa)	Mises equivalent stress (MPa)	Pressure (MPa)	Mises equivalent stress (MPa)	Pressure (MPa)	Mises equivalent stress (MPa)
30	60	931.4	90	946.3	120	953.7
54	60	926.7	90	952.4	120	961.2
96	60	941.2	90	959.1	120	965.7
195	60	943.5	90	965.7	120	974.3
825	60	946.2	90	969.3	120	986.7

After undergoing scientific validation, the C3D8 hexahedral element was employed to mesh the finite element model. Given the substantial stress and strain gradients in the corrosion zone, the area with corrosion was extracted, further divided, and locally refined to achieve the required accuracy. To enhance computational efficiency, the tubing body distant from the corrosion area was meshed using a sparse grid. For the P110S tubing, its axial length outside the corrosion regions is partitioned into 80 segments, the circumferential length is split into 40 sections, and the radial thickness is divided into 4 layers, as shown in Fig. 3c.

(3) Load and boundary conditions

The tubing is subjected to multiple loads including tubing weight, internal pressure, and annular pressure in an actual service environment. Among these, internal pressure has the most significant influence on tubing stress. Consequently, only the effects of internal pressure are paid great attention in the simulation while other loads are neglected. The uniform internal pressure is applied on the inner wall of corroded tubing, as shown in Fig. 3d. The displacement constraint is imposed on both ends of the corroded tubing [36], as shown in Fig. 3d.

(4) Stress-corrosion subroutine

At present, many scholars have conducted extensive research on stress corrosion, such as Li, Sun, and Cheng [37–39]. The methodologies have been proposed by Li, Sun, and Cheng including a relatively complex computational process (solving the stress distribution, calculating the electric field, and determining the local corrosion current density based on Gutman's mass transfer theory). Based on the Stress-Corrosion (SC) rate model proposed by Yang [40], as shown in Eq. (1), the customized subroutine (stress-corrosion subroutine) has been developed by using Fortran language and embedded into ABAQUS to simulate stress-corrosion interactions.

$$\lg V_{cr} = a \exp\left(b \frac{\sigma}{\sigma_y}\right) \tag{1}$$

where V_{cr} denotes the corrosion rate, mm/y; σ denotes the applied stress (i.e., the Von-Mises equivalent stress in the simulation), MPa; σ_y denotes the yield stress of the material, MPa; and a and b denote the electrochemical empirical parameters, where $a = -0.71557$ and $b = -0.69148$.

The realization of mechanical-chemical coupling includes three main processes based on the stress-corrosion subroutine as follows. Firstly, the corresponding Von-Mises equivalent stress σ is obtained by finite element analysis at the initial time step. Secondly, the local corrosion rate V_{cr} can be obtained based on the stress-corrosion rate model, and the displacement increment of the element nodes in the finite element model is driven by the corrosion rate to realize the dynamic update of the corrosion defect morphology. Finally, the updated morphology is used as the new initial condition and the stress field-corrosion rate-corrosion morphology is repeatedly updated based on the cyclic iteration, by which the dynamic evolution of corrosion morphology of tubing can be realized under multi-field coupling.

4 Model Validation

(1) Comparison with classical model

In this study, the effects of uniform corrosion defects with a size of 50 mm (axial) ∗ 50 mm (circumferential) ∗ 2 mm (depth) on the integrity of P110S and N80 tubing were investigated. The burst pressure was calculated by ASME B31 G [41], PCORRC [41], and DNV-RP-F101 [42], and compared with the finite element simulation results. The STATUSXFEM parameter (0–1.0) was used to quantitatively characterize the crack propagation state during the research process, which shows that the corrosion depth is the key factor affecting the residual strength. The results show that different evaluation models have good consistency with the simulation data, which provides a reliable basis for the safety evaluation of tubing with corrosion defects, the results are shown in Table 3 and Fig. 4.

Table 3: Comparison between simulation results and calculation results

Classical model		ASME B31G	PCORRC	DNV-RP-F101	Simulated result
Burst pressure/MPa	P110S	117.3	131.5	133.5	126.2
	N80	87.87	76.77	85.2	81.3

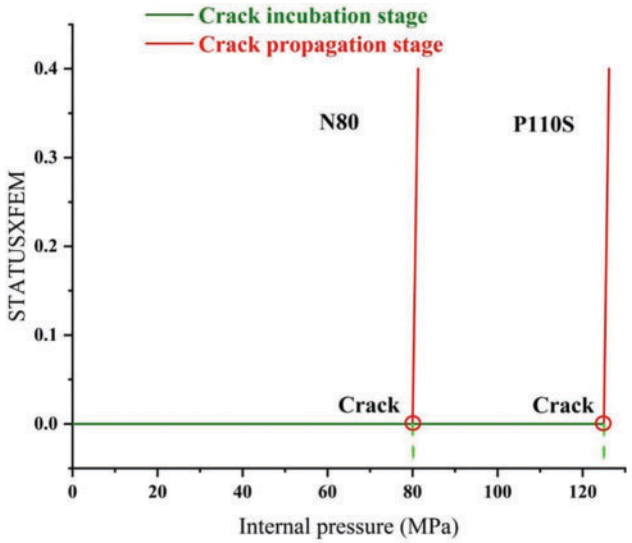

Figure 4: STATUSXFEM of P110S tubing with uniform corrosion under different internal pressure

For the P110S tubing, the comparison shows that the differences between the burst pressure of simulation results (126.2 MPa) and calculation results from the ASME B31G standard, PCORRC method, and DNV-RP-F101 standard are only 9.9, 8.3, and 6.3 MPa, respectively, and all the errors are less than 10%. Similarly, for the N80 tubing, the difference between simulation results and calculation results is only 6.57, 4.53, and 3.9 MPa, respectively. It demonstrates that the finite element model could be used to investigate the burst mechanical behavior of corroded tubing, and the simulation results are accurate and reliable.

(2) Comparison with experimental result

In this study, P110 tubing (outer diameter 73 mm, wall thickness 5.5 mm, yield strength 760 MPa, tensile strength 890 MPa) was used as the experimental material. The accuracy of the model was verified by comparing the simulation results of the finite element model with the experimental data of the burst pressure of the corroded tubing in Reference [43]. The simulation results show that the crack and blasting morphology of the T25/T26 corroded tubing are highly consistent with the experimental morphology [44], as shown in Fig. 5, and the error between the simulated value of the blasting pressure and the experimental data is less than 10%, as shown in Table 4. This shows that the finite element model has high accuracy and reliability, and is suitable for predicting the mechanical properties of corroded tubing.

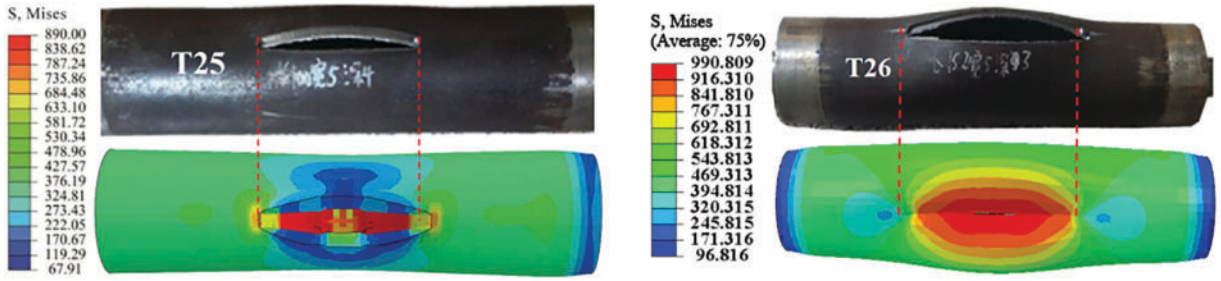

Figure 5: Comparison of simulation results and experimental results of T25 and T26 corrosion tubing

Table 4: Comparison of finite element simulation results with experimental results

Serial number	Corrosion length (mm)	Corrosion width (mm)	Corrosion depth (mm)	Experimental value (MPa)	Finite element value (MPa)
T25	100	5	4	37.6	41.2
T26	200	5	3	55.27	61.5

5 Study on the Mechanical Behavior of Tubing with Rectangular Corrosion

5.1 Affecting Factor of Mechanical Behavior

The mechanical behavior of corroded tubing is affected by many factors, such as operating pressure, corrosion defect depth, ambient temperature, corrosion time, circumferential length, and axial length, and the effect of those factors on mechanical behavior is determined by calculating the Von-Mises equivalent stress (VMES) and the volume loss rate is under specific conditions. The detailed simulation analysis is as follows.

5.1.1 Effect of Operating Pressure on Mechanical Behavior

A three-dimensional finite element model of tubing with rectangular corrosion defect (The circumferential corrosion length is 50 mm, and the axial corrosion length is 50 mm, the corrosion depth is 2.5 mm.) has been established. The service temperature is set to 60°C, and the service time is set to 2 years. The VMES and volume loss rate before and after tubing corrosion under different operating pressures of 30, 35, 40, 45, and 50 MPa have been simulated, as shown in Figs. 6 and 7.

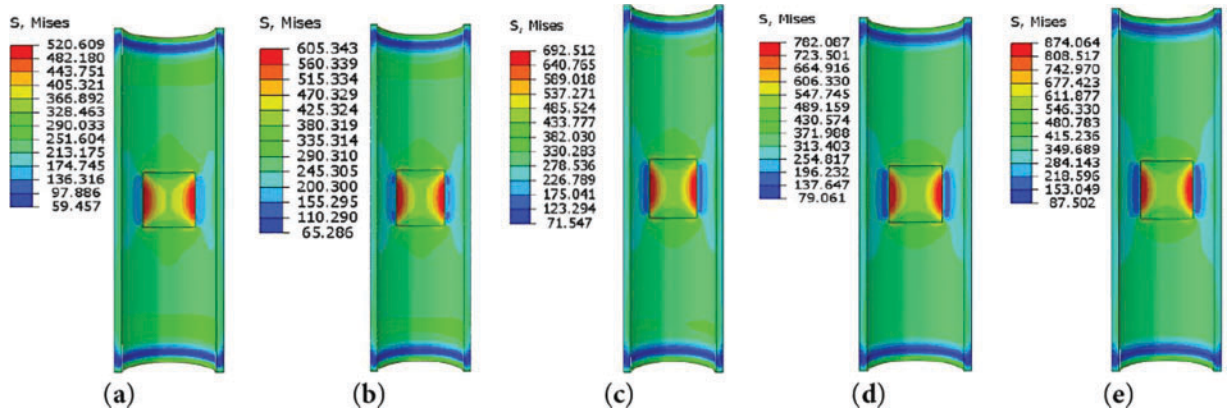

Figure 6: VMES of tubing under different operating pressure. (**a**) P_i = 30 MPa; (**b**) P_i = 35 MPa; (**c**) P_i = 40 MPa; (**d**) P_i = 45 MPa; (**e**) P_i = 50 MPa

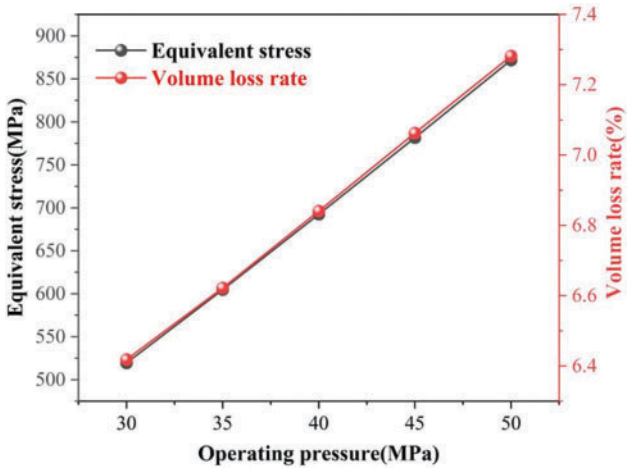

Figure 7: Volume loss rate of tubing under different operating pressure

Figs. 6 and 7 show that the corroded tubing is in the elastic deformation stage under different operating pressures because the maximum VMES (874 MPa) under operating pressures of 50 MPa is less than the yield strength (895 MPa), and the maximum VMES appears in the left and right sides of rectangular corrosion area, and the VMES and volume loss rate of tubing increases linearly with increase of operating pressure. The maximum VMES increases by 48.5% when the operating pressure ranges from 30 to 50 MPa, and the volume loss rate increases by 13.4% from 30 to 50 MPa, which demonstrates that the increasing operating pressure increases the VMES and aggravates the tubing corrosion.

5.1.2 Effect of Corrosion Morphology on Mechanical Behavior

(1) Influence of corrosion depth (L_d) on mechanical behavior

A three-dimensional finite element model of tubing with rectangular corrosion defect (The circumferential corrosion length is 50 mm, the axial corrosion length is 50 mm, and the corrosion depths are 1, 1.5, 2, 2.5, and 3 mm.) which has been established. The service temperature is set to 60°C, the service time is set to 2 years, and the operating pressure is set to 40 MPa. The VMES and volume loss rate before and after tubing corrosion under different corrosion depths of 1, 1.5, 2, 2.5, and 3 mm have been simulated, as shown in Figs. 8 and 9.

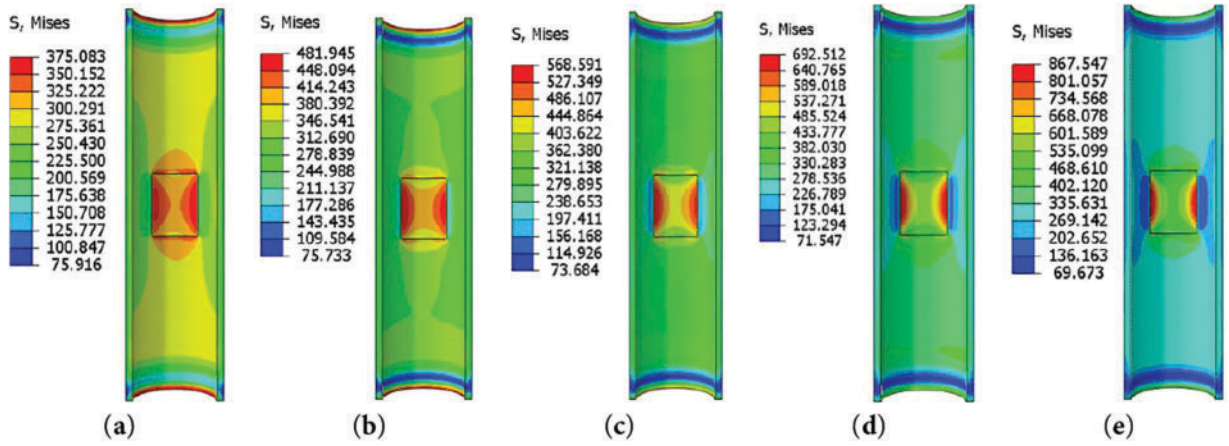

Figure 8: VMES of tubing under different corrosion depths. (**a**) L_d = 1 mm; (**b**) L_d = 1.5 mm; (**c**) L_d = 2 mm; (**d**) L_d = 2.5 mm; (**e**) L_d = 3 mm

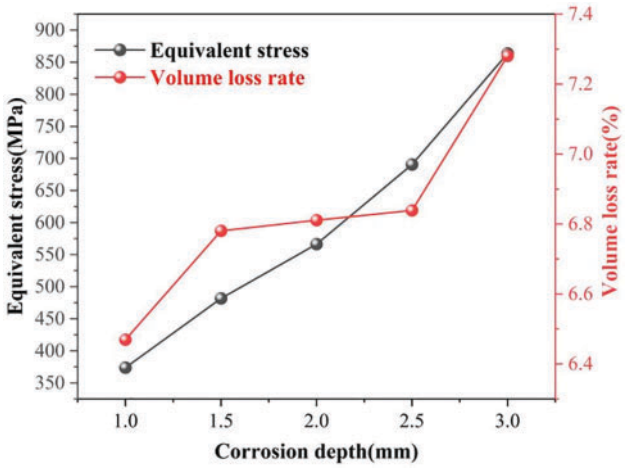

Figure 9: Volume loss rate of tubing under different corrosion depth

Figs. 8 and 9 show that the corroded tubing is in the elastic deformation stage under different corrosion depths because the maximum VMES (867 MPa) under a corrosion depth of 3.0 mm is less than the yield strength (895 MPa) of tubing material, and the maximum VMES also appears in the left and right sides of rectangular corrosion area, and the VMES and volume loss rate of tubing increases almost linearly with increase of corrosion depth. The maximum VMES increases by 131% when the corrosion depth ranges from

1.0 to 3.0 mm, and the volume loss rate increases by 12.6% from 1.0 to 3.0 mm, which demonstrates that the increasing VMES aggravates the tubing corrosion. Namely, stress and corrosion promote each other.

(2) Influence of circumferential corrosion length (L_h) on the mechanical behavior

Similarly, the service temperature is set to 60°C, the service time is set to 2 years, the operating pressure is set to 40 MPa, the corrosion depth is 3 mm, and the axial corrosion length is 50 mm. The VMES and volume loss rate before and after tubing corrosion under different circumferential corrosion lengths of 20, 25, 30, 35, and 40 mm have been simulated, as shown in Figs. 10 and 11.

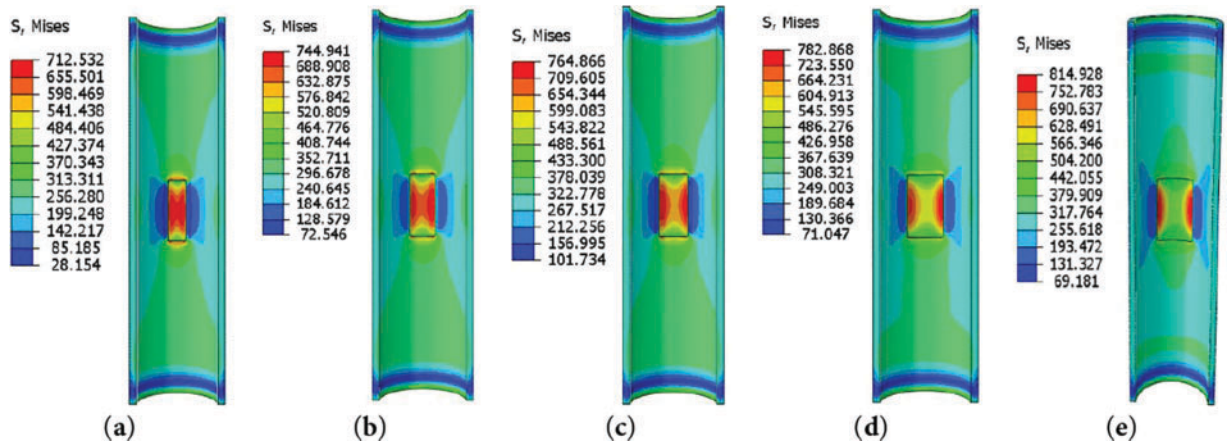

Figure 10: VMES of tubing under different loop corrosion lengths. (**a**) L_h = 20 mm; (**b**) L_h = 25 mm; (**c**) L_h = 30 mm; (**d**) L_h = 35 mm; (**e**) L_h = 40 mm

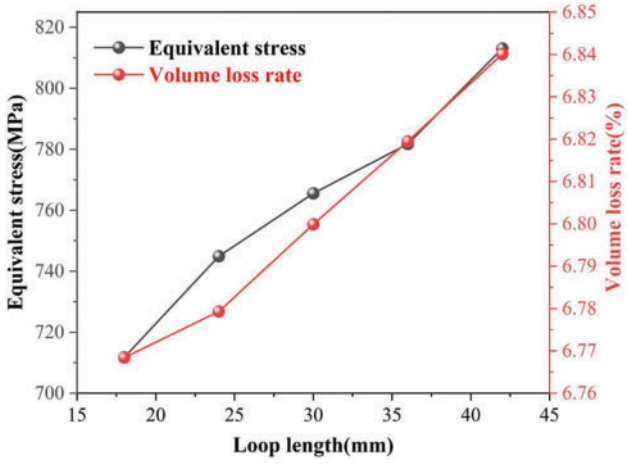

Figure 11: Volume loss rate of tubing under different loop length

Figs. 10 and 11 show that the corroded tubing is in the elastic deformation stage under different circumferential lengths because the maximum VMES (814 MPa) under corrosion depth of 3.0 mm is less than the yield strength (895 MPa) of tubing material, and the maximum VMES also mainly appears in the left and right sides of rectangular corrosion area, and the VMES and volume loss rate of tubing increases almost linearly with increase of corrosion depth too. However, the maximum VMES increases only by 14.3% when the circumferential length ranges from 20 to 40 mm, and the volume loss rate increases by 1.1% from

20 to 40 mm, which demonstrates that the stress and corrosion promote each other, but the circumferential length has a small effect on the VMES and corrosion of tubing.

(3) Influence of axial length (L_a) on the mechanical behavior

Similarly, the service temperature is set to 60°C, and the service time is set to 2 years, and the operating pressure is set to 40 MPa, and the corrosion depth is 3 mm, and the circumferential length is 50 mm. The VMES and volume loss rate before and after tubing corrosion under different axial corrosion lengths of 20, 25, 30, 35, and 40 mm have been simulated, as shown in Figs. 12 and 13.

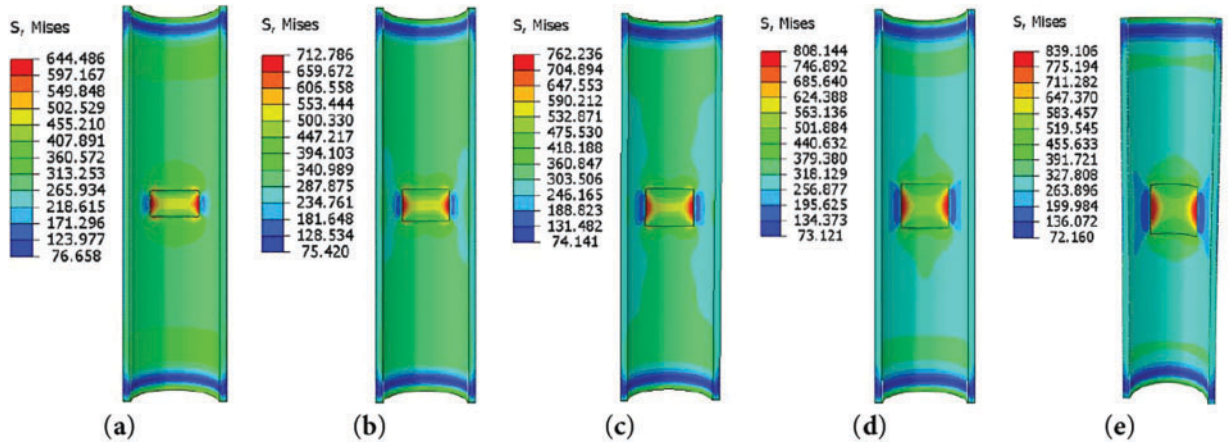

Figure 12: VMES of tubing under different axial lengths. (**a**) L_a = 20 mm; (**b**) L_a = 25 mm; (**c**) L_a = 30 mm; (**d**) L_a = 35 mm; (**e**) L_a = 40 mm

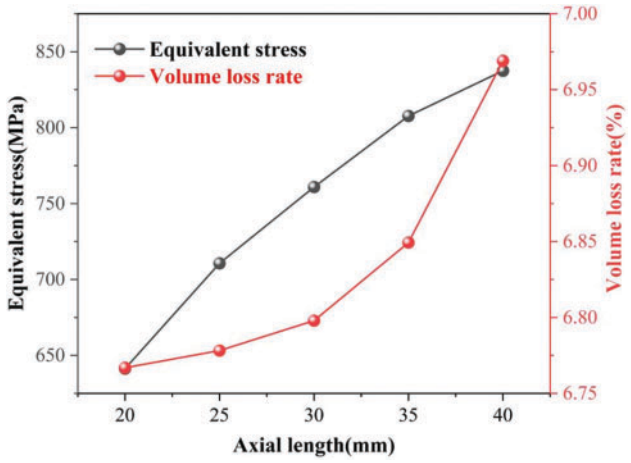

Figure 13: Volume loss rate of tubing under different axial length

Figs. 12 and 13 show that the corroded tubing is in the elastic deformation stage under different circumferential lengths because the maximum VMES (839 MPa) under corrosion depth of 3.0 mm is less than the yield strength (895 MPa) of tubing material, and the maximum VMES also appears in the left and right sides of rectangular corrosion area, and the VMES of tubing increases almost linearly with increase of axial length, but the volume loss rate of tubing increases non-linearly. The maximum VMES increases only by 30.3% when the axial length ranges from 20 to 40 mm, and the volume loss rate increases by 4.0% from

20 to 40 mm, which demonstrates that the stress and corrosion promote each other, but the axial length has a certain effect on the VMES and corrosion of tubing.

5.1.3 Effect of Service Temperature on Mechanical Behavior

A three-dimensional finite element model of tubing with rectangular corrosion defect (The circumferential corrosion length is 50 mm, and the axial corrosion length is 50 mm, the corrosion depth is 2.0 mm.) has been established. The service time is set to 2 years, and the operating pressure is set to 40 MPa. The VMES and volume loss rate before and after tubing corrosion under different service temperatures of 60°C, 75°C, 90°C, 105°C, and 120°C have been simulated, as shown in Figs. 14 and 15.

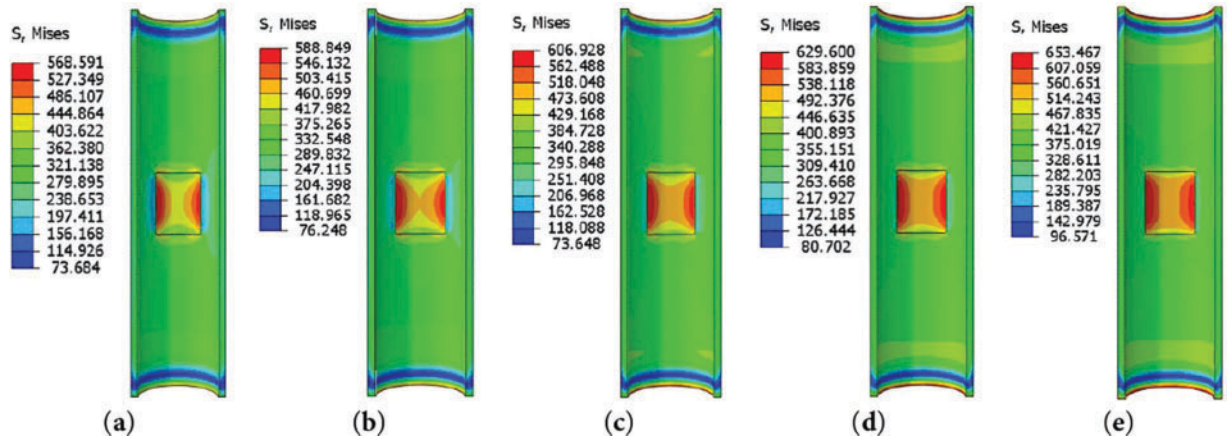

Figure 14: VMES under different service temperatures. (**a**) *Temp* = 60°C; (**b**) *Temp* = 75°C; (**c**) *Temp* = 90°C; (**d**) *Temp* = 105°C; (**e**) *Temp* = 120°C

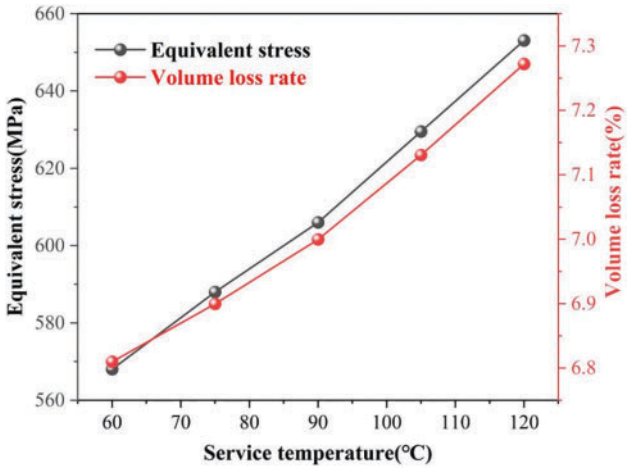

Figure 15: Volume loss rate of tubing under different service temperature

Figs. 14 and 15 show that the corroded tubing is in the elastic deformation stage under different circumferential lengths because the maximum VMES (653 MPa) under a service temperature of 120°C is much less than the yield strength (895 MPa) of tubing material, and the maximum VMES also appears in the left and right sides of rectangular corrosion area, and the VMES and volume loss rate of tubing

increases almost linearly with increase of service temperature. The maximum VMES increases only by 14.9% when the service temperature ranges from 60°C to 120°C, and the volume loss rate increases by 6.7% from 60°C to 120°C, which demonstrates that the temperature and corrosion promote each other, but the service temperature only has a certain effect on the VMES and corrosion of tubing.

5.1.4 Effect of Service Time on Mechanical Behavior

A three-dimensional finite element model of tubing with rectangular corrosion defect (The circumferential corrosion length is 50 mm, the axial corrosion length is 50 mm, and the corrosion depth is 2.0 mm.) has been established. The operating pressure is set to 40 MPa, and the service temperature is set to 60°C. The VMES and volume loss rate before and after tubing corrosion under different service times of two years, three years, four years, five years, and six years, have been simulated, as shown in Figs. 16 and 17.

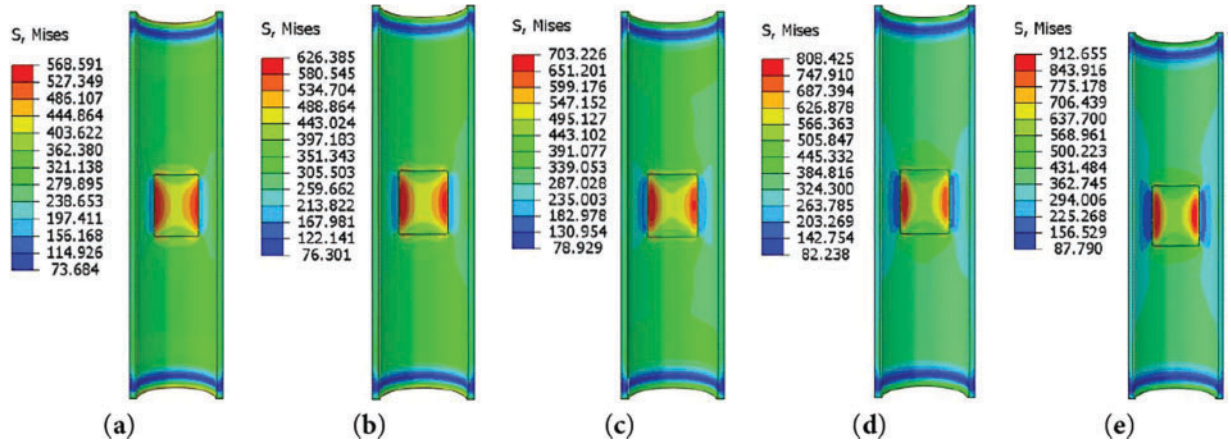

Figure 16: Von-Mises equivalent stress contours corresponding to different service times. (**a**) *Time* = 2 years; (**b**) *Time* = 3 years; (**c**) *Time* = 4 years; (**d**) *Time* = 5 years; (**e**) *Time* = 6 years

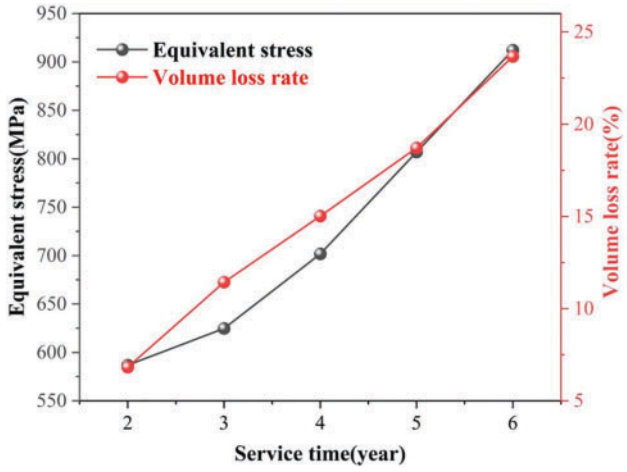

Figure 17: Volume loss rate of tubing under different service time

Figs. 14 and 15 show that the corroded tubing has successively gone through the elastic stage and the plastic stage, and it is in the elastic deformation stage when the service time is no more than five years, but it

is in the plastic deformation stage when the service time is more than five years because the maximum VMES (912 MPa) is more than the yield strength (895 MPa) of tubing material. Similarly, the maximum VMES also appears on the left and right sides of the rectangular corrosion area. The VMES and volume loss rate of tubing increas almost linearly with the increase in service time. The maximum VMES increases by 60.5% when the service service time is from 2 years to 6 years, and the volume loss rate increases by 264% from 2 years to 6 years. It is concluded that the corrosion morphology develops rapidly and causes great damage to the metal matrix with the increase in service time, which indicates that the service time has a serious influence on the tubing corrosion, and the service time and corrosion promote each other.

5.2 Grey Relational Analysis of Influencing Factors

The grey correlation analysis method is a systematic method for studying the degree of correlation between the reference sequence and comparison sequence based on the similarities and differences in their development trends. It quantifies the correlation degree between the reference sequence and comparison sequence by calculating the grey correlation coefficient R. In this paper, the corrosion depth, circumferential length, axial length, service temperature, service time, and operating pressure are defined as comparison sequence, and the volume loss rate is defined as reference sequence, and all the grey correlation coefficients (R1, R2, R3, R4, R5, R6) of comparison sequence have been calculated based on the simulation results, as shown in Table 5, by which the correlation degree between the reference sequence and comparison sequence can be analyzed.

Table 5: Grey correlation coefficient of comparison sequence

Type of corrosion	Influencing factors					
	Operating pressure R_1	**Corrosion depth R_2**	**Axial length R_3**	**Circumferential length R_4**	**Temperature R_5**	**Service time R_6**
Rectangular corrosion	0.953	0.947	0.868	0.859	0.757	0.753

It can be seen from Table 5 that the grey correlation coefficient R_1 of operating pressure is the largest, and the grey correlation coefficient R_6 corrosion time is the smallest, and the other are between them, which indicates that the operating pressure has the greatest influence on the mechanical behavior of the tubing, and the service time has the least influence.

5.3 Time-Varying Strength of Tubing under Different Corrosion Defects

5.3.1 Time-Varying Strength under Different Circumferential Corrosion Length

A three-dimensional mechanical model of tubing with rectangular corrosion defect (The axial corrosion length is 50 mm, and the corrosion depth is 3.0 mm.) has been established. The service temperature is set to 60°C, and the operating pressure is 70 MPa. The VMES of tubing under different circumferential corrosion lengths (20 and 40 mm) and service time (2 years and 4 years) have been simulated, as shown in Fig. 18.

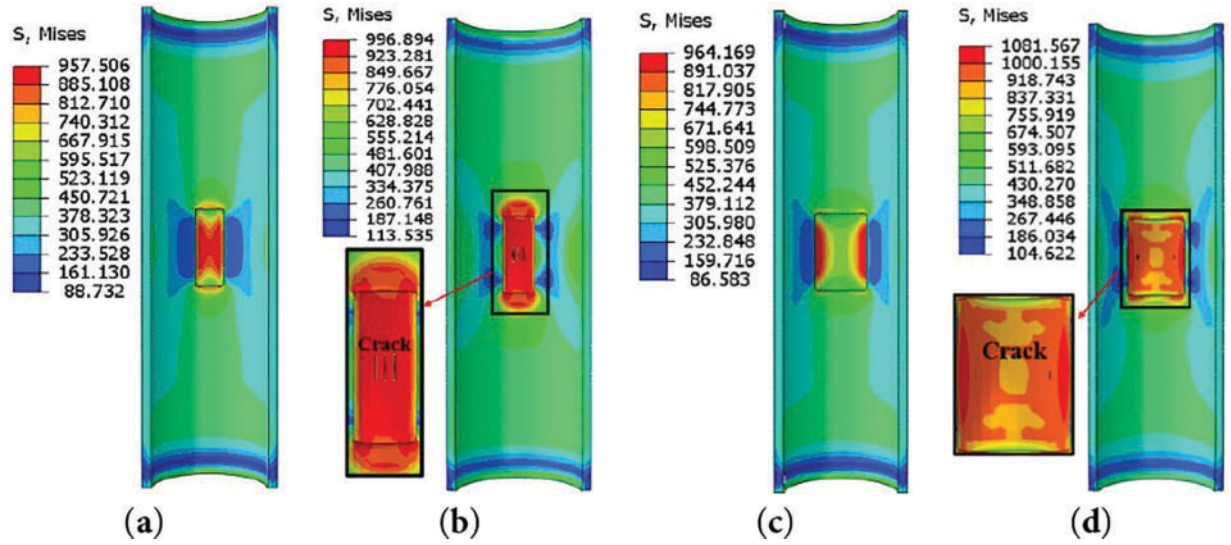

Figure 18: VMES of tubing under different circumferential corrosion lengths and service time. (**a**) L_h = 20 mm, *Time* = 2 years; (**b**) L_h = 20 mm, *Time* = 4 years; (**c**) L_h = 40 mm, *Time* = 2 years; (**d**) L_h = 40 mm, *Time* = 4 years

Fig. 18a,c shows that the maximum VMES (957 and 964 MPa) is greater than the yield strength (895 MPa) but less than the tensile strength (990 MPa) of the tubing material, which indicates that the tubing is in the plastic deformation stage, and its structure is intact without crack, but there is a certain degree of safety risk for the tubing such as deformation and burst failure when the service time is 2 years. Fig. 18b,d shows that the maximum VMES (996 and 1081 MPa) is greater than the yield strength (895 MPa) and tensile strength (990 MPa) of tubing material, and the longitudinal cracks appear obviously from the inner wall of tubing so that burst failure occurs, by which the service life of P110S tubing has been predicted under different circumferential corrosion lengths based on time step for crack initiation, as shown in Table 6. In addition, it can be seen from Fig. 18 that tubing has undergone severe plastic deformation so that the corrosion morphology extends outward resulting in an increase in the corrosion area.

Table 6: Prediction of service time for P110S tubing under different circumferential lengths

Circumferential length (mm)	Service time (Year)	Total time step	Time step for crack initiation (Year)	Service life (Year)
20	4	1	0.77	3.08
40	4	1	0.84	3.36

5.3.2 Time-Varying Strength under Different Axial Corrosion Lengths

A three-dimensional mechanical model of tubing with rectangular corrosion defect (The circumferential corrosion length is 50 mm, and the corrosion depth is 3.0 mm.) has been established. The service temperature is set to 60°C, and the operating pressure is 70 MPa. The VMES of tubing under different axial corrosion lengths (20 and 40 mm) and service time (2 years and 4 years) have been simulated, as shown in Fig. 19.

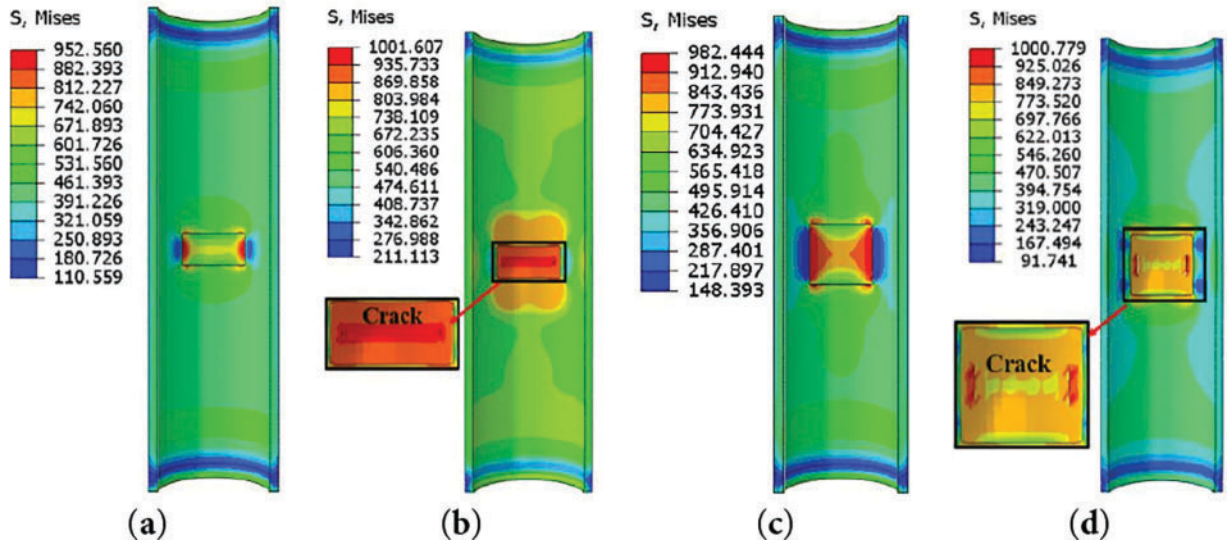

Figure 19: VMES of tubing under different axial corrosion lengths and service time. (**a**) *La* = 20 mm, *Time* = 2 years; (**b**) *La* = 20 mm, *Time* = 4 years; (**c**) *La* = 40 mm, *Time* = 2 years; (**d**) *La* = 40 mm, *Time* = 4 years

Fig. 19a,c shows that the maximum VMES (952 and 982 MPa) is greater than the yield strength (895 MPa) but less than the tensile strength (990 MPa) of the tubing material, which indicates that the tubing is in the plastic deformation stage, and its structure is intact without crack, but there is a certain degree of safety risk for the tubing such as deformation and burst failure when the service time is 2 years. However, in Fig. 19b,d, the maximum VMES (1001 and 1000 MPa) is greater than the yield strength (895 MPa) and tensile strength (990 MPa) of the tubing material, and the longitudinal cracks appear obviously from the inner wall of tubing so that burst failure occurs, by which the service life of P110S tubing has been predicted under different axial corrosion lengths by analyzing the initial crack-related parameters, as shown in Table 7. Similarly, it can be seen from Fig. 19 that tubing has undergone severe plastic deformation so that the corrosion morphology extends outward and the corrosion area increases.

Table 7: Prediction of P110S tubing service life under different axial lengths

Axial length (mm)	Service time (Year)	Total time step	Time step for crack initiation (Year)	Service life (Year)
20	4	1	0.82	3.28
40	4	1	0.76	3.04

5.3.3 Time-Varying Strength under Different Corrosion Depths

A three-dimensional mechanical model of tubing with rectangular corrosion defect (The circumferential corrosion length is 50 mm, and the axial corrosion length is 50 mm.) has been established. The service temperature is set to 60°C, and the operating pressure is 65 MPa. The VMES of tubing under different corrosion depths (2.0 and 3.0 mm) and service time (2 years and 4 years) have been simulated, as shown in Fig. 20.

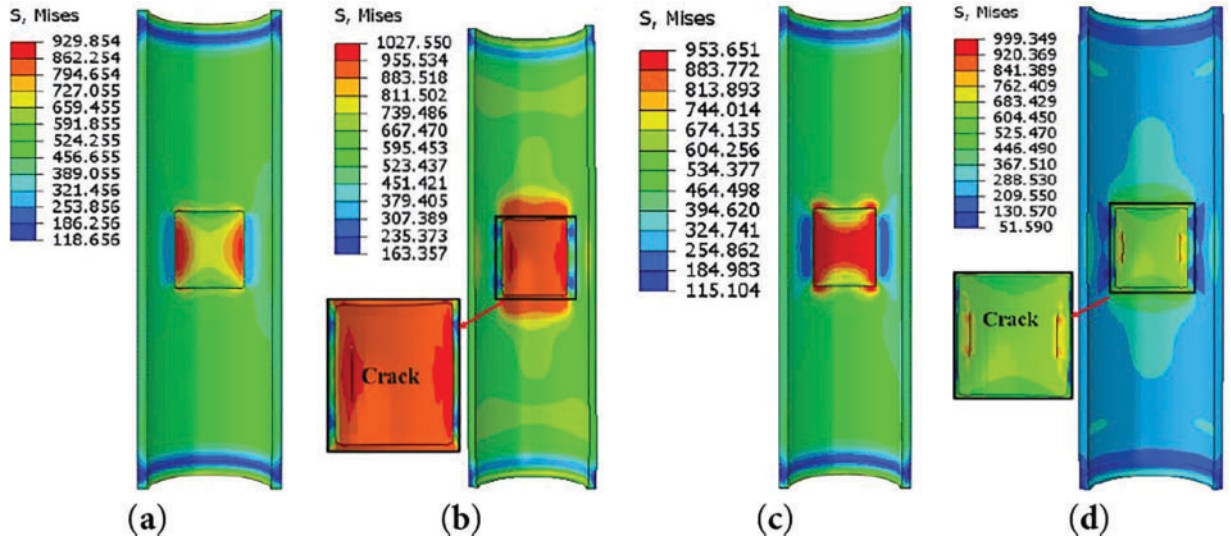

Figure 20: VMES of tubing under different corrosion depths and service time. (**a**) L_d = 2 mm, *Time* = 2 years; (**b**) L_d = 2 mm, *Time* = 4 years; (**c**) L_d = 3 mm, *Time* = 2 years; (**d**) L_d = 3 mm, *Time* = 4 years

Fig. 20a,c shows that the maximum VMES (929 and 953 MPa) is greater than the yield strength (895 MPa) but less than the tensile strength (990 MPa) of the tubing material, which indicates that the tubing is in the plastic deformation stage, and its structure is intact without crack, but there is a certain degree of safety risk for the tubing such as deformation and burst failure when the service time is 2 years. However, Fig. 20a,c shows that the maximum VMES (1027 and 999 MPa) is greater than the yield strength (895 MPa) and tensile strength (990 MPa) of tubing material, and the longitudinal cracks appear obviously from the inner wall of tubing so that burst failure occurs, by which the service life of P110S tubing has been predicted under different circumferential corrosion lengths based on time step for crack initiation, as shown in Table 8. In addition, it can be seen from Fig. 20 tubing has undergone severe plastic deformation so that the corrosion area extends and increases.

Table 8: Prediction of the service life of P110S tubing under different corrosion depths

Corrosion depth (mm)	Service time (Year)	Total time step	Time step for crack initiation (Year)	Service life (Year)
2	4	1	0.85	3.40
3	4	1	0.62	2.48

6 Discussions

In this paper, the effects of defect morphology (circumferential corrosion length, axial corrosion length, corrosion depth), service temperature, and operating pressure on the mechanical behavior of tubing have been investigated. It has been found that the VMES at the corrosion defect varies to varying degrees with the changes in morphology, service temperatures, and operating pressures. The degree of correlation between operating pressure and VMES is the highest, the next is corrosion depth, and the service time is the lowest. In other words, the operating pressure and corrosion depth have the greatest contribution to tubing failure. As a

result, Oil and gas engineers should attach great importance to monitoring operating pressure and corrosion depth, along with related production parameters under actual working conditions.

At the same time, it is necessary to maintain the tubing section with deep defects in a timely manner. Furthermore, accurately predicting the service time of corroded tubing is crucial for ensuring production safety. For solving this problem, the time-varying strength could be simulated based on the three-dimensional mechanical model proposed by this paper, and the service life of corroded tubing under different service environments could be obtained, this enables engineers to develop maintenance plans based on the predicted lifespan.

However, the research in this paper has some limitations. Firstly, the ranges of the current temperature, pressure, and service time are limited, so the effect of the higher temperatures, pressures, service time, and its coupling on the mechanical behavior of tubing requires further investigation based on the experiment and simulation because the service environment is becoming increasingly harsh. Secondly, the three-dimensional finite element model needs to be improved for tubing made of new materials, such as titanium alloy. Finally, the three-dimensional finite element model is unsuitable for analyzing the mechanical behavior of tubing with pitting and mixed corrosion.

7 Conclusions

(1) Mechanical and thermodynamic parameters of P110S tubing material have been measured, and the three-dimensional thermal-mechanical-chemical multi-field coupling mechanical model of P110S tubing with rectangular corrosion defect has been established based on XFEM by developing stress-corrosion subroutine with due consideration of the geometric non-linearity caused by large deformation, and its accuracy and reliability are validated by using calculation results form the classic standard and full-scale burst experimental data.

(2) Effects of operating pressure, corrosion depth, circumferential/axial lengths, service temperature, and service time on the mechanical behavior and corrosion rate of tubing have been obtained, by which the sensitivity analysis of the corrosion rate and VMES has been conducted by using the grey relational analysis method. The results show that the operating pressure has the greatest impact on the corrosion rate and VMES of the tubing, and the service time has the least impact corrosion rate and VMES.

(3) Elastic-plastic deformation, crack propagation, and burst failure behavior of tubing under different corrosion defects have been simulated, by which the effect of circumferential corrosion length and axial corrosion length as well as corrosion depth on time-varying strength of tubing has been obtained, and the service life has been predicted.

Acknowledgement: Not applicable.

Funding Statement: The authors received no specific funding for this study.

Author Contributions: Yi Huang: Conceptualization, Modeling, Investigation, Formal analysis, Writing—original draft. Ming Luo and Zhujun Li: Modeling, Data curation, Writing—original draft. Donglei Jiang and Ping Xiao: Data curation, Investigation, Writing—review & editing. Mingyuan Yao and Jia He: Simulation, Writing—review & editing. All authors reviewed the results and approved the final version of the manuscript.

Availability of Data and Materials: The data that support the findings of this study are available from the corresponding author upon reasonable request.

Ethics Approval: Not applicable.

Conflicts of Interest: The authors declare no conflicts of interest to report regarding the present study.

References

1. Cai AF, Qian C, Zhu J, Nie XZ, Cheng X, Yang G, et al. Mechanical characterization of thin-walled homogeneous hot plate under thermal coupling. Vac Cryog. 2024;30(2):157–65. (In Chinese). doi:10.12446/j.issn.1006-7086.2024.02.008.
2. Zhang HZ, Zhang CG, Zheng L. Development status and trend of continuous oil pipe. Welded Pipe. 2022;45:25–31. (In Chinese).
3. Zhong CW. Analysis of ultimate bearing capacity of composite repaired pipeline considering temperature and material degradation [dissertation]. Beijing, China: China University of Petroleum; 2018. (In Chinese).
4. Sedmak A, Arsić M, Šarkoćević Ž., Medjo B, Rakin M, Arsić D, et al. Remaining strength of API J55 steel casing pipes damaged by corrosion. Int J Press Vessels Pip. 2020;188:104230. doi:10.1016/j.ijpvp.2020.104230.
5. Mondal BC, Dhar AS. Burst pressure assessment of corroded pipelines using fracture mechanics criterion. Eng Fail Anal. 2019;104:139–53. doi:10.1016/j.engfailanal.2019.05.033.
6. Mondal BC, Dhar AS. Burst pressure of corroded pipelines considering combined axial forces and bending moments. Eng Struct. 2019;186:43–51. doi:10.1016/j.engstruct.2019.02.010.
7. Fahed M, Barsoum I, Alfantazi A, Islam MD. Burst pressure prediction of pipes with internal corrosion defects. J Press Vessel Technol. 2020;142(3):031801. doi:10.1115/1.4045886.
8. Heggab A, El-Nemr A, El Aghoury IM. Numerical sensitivity analysis of corroded pipes and burst pressure prediction using finite element modeling. Int J Press Vessels Pip. 2023;202:104906. doi:10.1016/j.ijpvp.2023.104906.
9. Okodi A, Lin M, Yoosef-Ghodsi N, Kainat M, Hassanien S, Adeeb S. Crack propagation and burst pressure of longitudinally cracked pipelines using extended finite element method. Int J Press Vessels Pip. 2020;184:104115. doi:10.1016/j.ijpvp.2020.104115.
10. González-Arévalo NE, Díaz-Cruz M, Velázquez JC, Cervantes-Tobón A, Carrillo X, García-Núñez SJ, et al. Failure pressure estimation for cracked aged and unaged pipelines using finite element method. Results Eng. 2025;26:104621. doi:10.1016/j.rineng.2025.104621.
11. Mansour MM, Salman HS, Lafta AM, Nashee SR, Shkarah AJ. Simulation analysis of protection oil pipe in platform to reduced corrosion and erosion defect with sustainability technique. Math Model Eng Probl. 2024;11(5):1171–8. doi:10.18280/mmep.110505.
12. Mondal BC, Dhar AS. Investigation of the burst pressure of a pipeline with an inclined corrosion defect using FE analysis. J Pipeline Syst Eng Pract. 2025;16(2):04025015. doi:10.1061/jpsea2.pseng-1803.
13. Cao H, Yang QQ. Stress analysis of tubings with combined corrosion defects. Shandong Chem Ind. 2021;50(24):176–8. (In Chinese).
14. Zhao HY, Yang ZG, Liang X, Zhu XH. Simulation modeling and test on residual strength for corroded pipeline. Res Explor Lab. 2021;40(12):18–22. (In Chinese). doi:10.19927/j.cnki.syyt.2021.12.005.
15. D'Aguiar SCM, de Siqueira Motta R, Afonso SMB. An investigation on the collapse response of subsea pipelines with interacting corrosion defects. Eng Struct. 2024;321:118911. doi:10.1016/j.engstruct.2024.118911.
16. Silva R, Zhou W. Investigation of the defect width effect on the burst capacity of composite-repaired pipelines with corrosion defects using finite element analysis. J Press Vessel Technol. 2024;146(1):011201. doi:10.1115/1.4063889.
17. Kere KJ, Huang Q. Development of a probabilistic interaction rule and failure pressure model for pipelines with a colony of corrosion defects. J Pipeline Syst Eng Pract. 2025;16(2):04025004. doi:10.1061/jpsea2.pseng-1714.
18. Chen YF, Hou FH, Lang YM, Gao MD, Zhang Y, Xia TJ, et al. Calculation method of pressure collapse of submarine pipeline with corrosion defects. China Offshore Oil Gas. 2021;33(5):182–8. (In Chinese). doi:10.11935/j.issn.1673-1506.2021.05.023.
19. Capula-Colindres S, Terán G, Velázquez JC, Caballero-Rosas A, Torres-Santillán E, Angeles-Herrera D. Mechanical behavior of X60 pipelines containing pitting corrosion defects based on finite element method. Forces Mech. 2024;16:100278. doi:10.1016/j.finmec.2024.100278.
20. Ghelloudj O, Zelmati D, Ramoul CE, Gharbi A, Ayad A, Aoun ID, et al. Reliability assessment of pipeline steel under corrosion defect. Mater Today Proc. 2023;86:107. doi:10.1016/j.matpr.2023.05.212.

21. Olatunde M, Sriramula S, Siddiq MA, Akisanya AR. An investigation on the effect of widespread internal corrosion defects on the collapse pressure of subsea pipelines. Ocean Eng. 2023;287:115926. doi:10.1016/j.oceaneng.2023.115926.
22. Hosseinzadeh S, Bahaari M, Abyani M, Taheri M. Data-driven remaining useful life estimation of subsea pipelines under effect of interacting corrosion defects. Appl Ocean Res. 2025;155:104438. doi:10.1016/j.apor.2025.104438.
23. Shen YJ. Study on residual strength of high steel grade oil and gas pipelines with double corrosion defects. Pet Pipes Instrum. 2024;10(1):57–62. (In Chinese).
24. Mahmoodian M, Li CQ. Failure assessment and safe life prediction of corroded oil and gas pipelines. J Petrol Sci Eng. 2017;151:434–8. doi:10.1016/j.petrol.2016.12.029.
25. Soares E, Bruère VM, Afonso SMB, Willmersdorf RB, Lyra PRM, Bouchonneau N. Structural integrity analysis of pipelines with interacting corrosion defects by multiphysics modeling. Eng Fail Anal. 2019;97:91–102. doi:10.1016/j.engfailanal.2019.01.009.
26. Feki MS, Zghal S, Koubaa S, Bouaziz Z, Abdelmoula R. 3D finite element model for simulation of mechanical and electrochemical effects on corrosion defect of pipeline. In: Proceedings of the 10th Conference on Design and Modeling of Mechanical Systems, CMSM'2023; 2023 Dec 18–20; Hammamet, Tunisia. doi:10.1007/978-3-031-67152-4_13.
27. Qin G, Huang Y, Wang Y, Frank Cheng Y. Pipeline condition assessment and finite element modeling of mechano-electrochemical interaction between corrosion defects with varied orientations on pipelines. Tunn Undergr Space Technol. 2023;136:105101. doi:10.1016/j.tust.2023.105101.
28. Chen ZF, Huang Y, Wang W, Wang Y. Consistency analysis of burst pressure in corroded pipelines. J Press Vessel Technol. 2025;147(1):014501. doi:10.1115/1.4066906.
29. Deng K, Zhou N, Lin Y, Yan X, Luo Z, Yan R, et al. Study on residual strength and life prediction of corroded tubing based on thermal-mechanical coupling XFEM. Ocean Eng. 2022;255:111450. doi:10.1016/j.oceaneng.2022.111450.
30. Kiefner JF, Vieth PH. A modified criterion for evaluating the remaining strength of corroded pipe. Richland, WA, USA: Battelle Memorial Institute; 1989.
31. Stephens DR, Leis BN. Development of an alternative criterion for residual strength of corrosion defects in moderate- to high-toughness pipe. In: Proceedings of the 2000 3rd International Pipeline Conference; 2000 Oct 1–5; Calgary, AB, Canada. doi:10.1115/ipc2000-192.
32. Freire JL, Benjamin AC, Vieira RD, Diniz JL. Burst strength of pipeline test specimens containing longitudinal or circumferential corrosion defects. In: Proceedings of the 2011 Annual Conference on Experimental and Applied Mechanics; 2011 Jun 13–16; Uncasville, CT, USA. doi:10.1007/978-1-4614-0222-0_59.
33. Zhang Y. Preparation and corrosion behavior of Ni-W/TiN coated X52 pipeline steel [dissertation]. Daqing, China: Northeast Petroleum University; 2022. (In Chinese).
34. Huang Y, Song SH, Xu J, Li YX. Stress analysis of elliptical tubes with volumetric defects under internal pressure. Ordnance Mater Sci Eng. 2020;43(5):453–75. (In Chinese).
35. API 579. Fitness-for-service. Washington, DC, USA: American Petroleum Institute; 2007.
36. Huang KY. Influencing factors of interference between corrosion defects in the inner and outer wall of oil & gas transportation pipelines. Surf Technol. 2020;49(3):199–204. (In Chinese). doi:10.1007/s12182-019-00365-5.
37. Sun J, Cheng YF. Modelling of mechano-electrochemical interaction of multiple longitudinally aligned corrosion defects on oil/gas pipelines. Eng Struct. 2019;190:9–19. doi:10.1016/j.engstruct.2019.04.010.
38. Li M, Liu Z, Zhao Y, Zhou Y, Huang P, Li X, et al. Effects of corrosion defect and tensile load on injection pipe burst in CO_2 flooding. J Hazard Mater. 2019;366:65–77. doi:10.1016/j.jhazmat.2018.11.089.
39. Wang H, Yu Y, Xu Y, Gao J. A unified model and simulation method for elastoplastic stress–erosion interaction. Tribol Int. 2024;191:109111. doi:10.1016/j.triboint.2023.109111.
40. Huang Y, Zhang P, Qin G. Investigation by numerical modeling of the mechano-electrochemical interaction at a dent-corrosion defect on pipelines. Ocean Eng. 2022;256:111402. doi:10.1016/j.oceaneng.2022.111402.
41. Ma B, Shuai J, Wang J, Han K. Analysis on the latest assessment criteria of ASME B31G-2009 for the remaining strength of corroded pipelines. J Fail Anal Prev. 2011;11(6):666–71. doi:10.1007/s11668-011-9490-8.

42. Noor N, Ozman N, Yahaya N. Deterministic prediction of corroding pipeline remaining strength in marine environment using DNV RP-F101 (Part A). J Sustain Sci Manage. 2011;6(1):69–78.
43. Hu Z, Hua L, Liu J, Min S, Li C, Wu F. Numerical simulation and experimental verification of random pitting corrosion characteristics. Ocean Eng. 2021;240:110000. doi:10.1016/j.oceaneng.2021.110000.
44. Wang H, Yu Y, Xu W, Li Z, Yu S. Time-variant burst strength of pipe with corrosion defects considering mechano-electrochemical interaction. Thin Walled Struct. 2021;169:108479. doi:10.1016/j.tws.2021.108479.